A Journal of the Gesellschaft Deutscher Chemiker

Angewandte International Edition GDCh Chemie

www.angewandte.org

Accepted Article

Title: Digital and Tunable Genetically Encoded Tension Sensors Based on Engineered Coiled-Coils

Authors: Shuhong Liu, Jinchan Liu, Alexander Foote, Hiroaki Ogasawara, Sarah Al Abdullatif, Victor S. Batista, and Khalid Salaita

To be cited as: *Angew. Chem. Int. Ed.* **2025**, e202407359

Link to VoR: https://doi.org/10.1002/anie.202407359

WILEY VCH

10.1002/anie.202407359

WILEY VCH

RESEARCH ARTICLE

Digital and Tunable Genetically Encoded Tension Sensors Based on Engineered Coiled-Coils

Shuhong Liu[a], Jinchan Liu[c], Alexander Foote[a], Hiroaki Ogasawara[a], Sarah Al Abdullatif[a], Victor S. Batista[d], and Khalid Salaita*[a, b]

[a] S. Liu, A. Foote, H. Ogasawara, S. Al Abdullatif, Prof. K. Salaita
Department of Chemistry
Emory University
Atlanta, Georgia 30322, United States
E-mail: k.salaita@emory.edu

[b] Prof. K. Salaita
Wallace H. Coulter Department of Biomedical Engineering
Georgia Institute of Technology and Emory University
Atlanta, Georgia 30322, United States

[c] J. Liu
Department of Molecular Biophysics and Biochemistry
Yale University
New Haven, Connecticut 06520, United States

[d] Prof. V. S. Batista
Department of Chemistry
Yale University
New Haven, Connecticut 06520, United States

Supporting information for this article is given via a link at the end of the document.

Abstract: Genetically encoded tension sensors (GETSs) allow for quantifying forces experienced by intracellular proteins involved in mechanotransduction. The vast majority of GETSs are comprised of a FRET pair flanking an elastic "spring-like" domain that gradually extends in response to force. Because of ensemble averaging, the FRET signal generated by such analog sensors conceals forces that deviate from the average, and hence it is unknown if a subset of proteins experience greater magnitudes of force. We address this problem by developing digital GETSs comprised of coiled-coils (CCs) with tunable mechanical thresholds. We validate the mechanical response of CC digital probes using thermodynamic stability prediction, AlphaFold2 modeling, steered molecular dynamics simulations, and single molecule force microscopy. Live cell measurements using optimized CC tension sensors that are inserted into vinculin demonstrate that 13% of this mechanosensor experiences forces > 9.9 pN within focal adhesions. This reveals greater magnitudes of vinculin force than had previously been reported and demonstrates that coiled-coil tension sensors enable more facile and precise tension measurements in living systems.

Introduction

Mechanical forces are essential for regulating a vast array of cellular processes that range from cell differentiation[1] and migration,[2] to proliferation.[3] Cells can sense and respond to mechanical cues through force sensing proteins that assemble within multi-protein complexes and are often associated with the cytoskeleton. One prominent example is the focal adhesion (FA) that includes hundreds of proteins, such as vinculin, integrins, and talin, which are mechanosensitive and involved in linking the extracellular matrix (ECM) to the cellular cytoskeleton. Over the past decade, a variety of molecular tension sensors (MTSs) have been developed to measure the forces experienced in cells.[4-11] The fundamental design principle for MTSs is to flank an extendable "spring element" with a donor/acceptor fluorophore pair and then to detect its extension using Förster resonance energy transfer (FRET). Force-induced extension of the linker will increase the distance between the fluorophore and quencher, thus generating a FRET response quantified using conventional fluorescence microscopy, the workhorse tool of cell biology.

Many types of extendable materials have been used in MTSs, such as polyethylene glycol (PEG) entropic springs, [5,6] proteins,[7] peptides,[8-10] as well as folded nucleic acids.[11] MTSs with entropic spring linkers behave like an analog sensor, where the distance between fluorophores increases gradually in response to the external force *(F),* and hence each MTS generates a FRET signal in response to *F* (**Scheme 1a**). Analog sensors are limited when analyzing ensemble averages of FRET signal because the average conceals the precise value of *F* for individual events. In other words, signal averaging obscures less frequent *F* values that differ from the average. There are two possible solutions to

10.1002/anie.202407359

the ensemble averaging problem. The first is the use of single molecule imaging, and this was demonstrated by *Tan et al. 2020* and *Matsubara et al. 2023* with extracellular tension probes.[12,13] However, this is highly challenging when using genetically encoded tension sensors (GETSs) due to the difficulty of controlling fluorophore concentration, weak brightness, limited photostability, and large autofluorescence background.[14] A second approach to address the issue of ensemble averaging requires development of tension sensors that show a binary response to applied force. In this situation, the ensemble signal of a digital sensor is linearly proportional to the fraction of unfolded sensors. Several GETSs with different force-response ranges have been developed but none display sharp digital-like transitions. Those include the 40 amino acid (aa)-long flagelliform peptide (F40), 35-aa-long villin headpiece peptide (HP) and stabilized HP (HPst).[8,15] Such GETSs have been widely used in mechanobiology, and their force responses display gradual transitions with a width of 8-10 pN.[9] The most near-digital GETSs uses a ferredoxin-like (FL) linker peptide, which shows an unfolding transition 3-6 pN wide.[9] However, the problem with existing GETSs is that their response is difficult to predict and secondly it is not possible to rationally tune their force responses. Thus, there is a need to create a digital GETS with tunable responses that could allow mapping of sub-populations of proteins experiencing specific force magnitudes.

We investigated coiled-coil (CC) dimers as the force-sensing element in GETS due to their facile programmability which is akin to that of DNA.[16] Indeed, CCs are now being used to construct complex 3D structures using DNA-origami-like rules.[17] CCs are heptad repeats in which their peptide residue pairings are mainly driven by hydrophobic and electrostatic interactions at positions “a:d” and “e:g”, respectively either in a parallel or an antiparallel orientation (**Scheme 1b**).[16] By tuning the hydrophobicity in “a”, “d” positions and the electric charge of “e”, “g” residues, the pairing stability can be engineered according to empirical prediction.[18,19] Unlike linker materials that use elastic spring (ELP) like peptides, the a-helical CCs primarily adopts two conformations, folded and unfolded, leading to one major energy barrier for their unfolding.[20-22] Therefore, CC motifs provide a nearly ideal two-state binary force response, which has been calibrated in past studies with a wide range of force responses depending on their sequences.[22-26]

Here, we leverage the tunability and binary conformational transition of CCs to develop a CC-based GETS to visualize vinculin tension during cell adhesion. We created and tested a library of vinculin CC tension sensors (CCTSs) with a range of thermodynamic and mechanical stabilities and also created parallel control constructs that are force-insensitive (**Scheme 1c,d**). The relative mechanical stability of this library was investigated using AlphaFold2, the CCBuilder 2.0 thermodynamic prediction tool, and steered molecular dynamics (SMD), and these results were compared against single-molecule force spectroscopy analysis. Cell measurements showed that fine-tuning of CC stability is required to achieve a desirable dynamic range and sensitivity of the CCTS. The work led to identification of CC motifs that are mechanically matched to the forces transmitted across vinculin. Importantly, we found that ~13% of vinculin at focal adhesion experiences F >9.9 pN at 4 hr time point after seeding confirming the heterogeneity of force distribution and greater magnitudes of force than that had been reported previously. Finally, direct comparison of the optimized CCTS against that of the optimized ELP tension sensor (opt-VinTS) showed advantages of CCTS in terms of greater baseline FRET and response to a wider range of force magnitudes revealing the heterogeneous magnitudes of forces in cells.

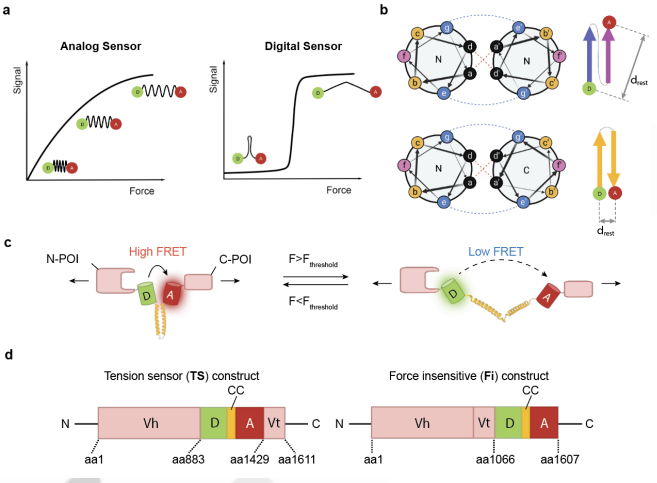

Scheme 1. CC-based digital GETS. (a) Hypothetical plots comparing the response of analog (left) and digital (right) sensors. (b) Helical wheel and arrow diagrams of parallel (top) and antiparallel (bottom) CCs. Gray arrow indicates donor-acceptor distance at rest (d_{rest}) for each geometry. Note that a smaller d_{rest} is most desirable to maximize FRET change in response to force. (c) Design of CC tension sensor (CCTS) to detect forces transmitted across protein of interest (POI). When F is lower than the threshold, the probe shows high FRET signal, but when F exceeds the threshold, the CC unfolds and the probe shows low FRET signal. (d) Plasmid maps showing the design of the CCTS inserted between vinculin head (Vh) and tail (Vt) domains (left) and force insensitive control construct with CCTS attached at the C-terminus of vinculin (right). *D* = donor and *A* = acceptor.

Results and Discussion

Design and Geometry Considerations for Creating a Vinculin CCTS

In principle, one can design CC sensors in a parallel or antiparallel geometry (**Scheme 1b**). The antiparallel geometry is preferred to maximize the S/N of the FRET response since this geometry minimizes donor-acceptor distance at rest and maximizes separation upon mechanical unfolding (**Scheme 1b,c**). Nonetheless, we created and inserted antiparallel and parallel CCs into vinculin and found that both types of CCs maintain vinculin activity as measured by quantifying cell adhesion area in vinculin null MEFs (**Supplementary Note 1, Figure S1**). Note that parallel CCs with a short linker that prevents intramolecular CC folding generated condensates that suppressed cell spreading. This observation along with the predicted improvement in S/N led us to pursue the antiparallel CC for the design of the vinculin TS. Notably, Ren et al. demonstrated that CC dimers in both parallel and antiparallel geometries form protein condensates in yeast

10.1002/anie.202407359

upon experiencing sufficient unfolding forces,[23] and this precedent would have suggested the vinculin CCs would inhibit vinculin activity. However, in our hands, the antiparallel CC vinculin constructs were functional and did not display condensate formation (**Figure S1**), likely due to the highly oriented assembly of vinculin within FAs that prevent intermolecular binding of opened antiparallel CCs.

Because we did not know *a priori* which CC is stable at rest and unfolds due to vinculin tension, we designed a series of CC domains with varying stability. The most effective way to dampen CC stability is to shorten the length of hydrophobic domain, which could be achieved by either reducing the number of heptad repeats or replacing the amino acids at "a", "d" positions with hydrophilic residues (**Scheme 1b**).[26] While changing the number of heptads is facile, we avoided this approach to maintain nearly identical donor-acceptor distance in the mechanically unfolded state and thus allowing the use of FRET to quantify the performance of different CC mutants. Therefore, we replaced leucine pairs with the more polar serine pairs starting from the loop side of CC domain. Specifically, we investigated CC-S_0, CC-S_1, CC-S_2, CC-S_4 and CC-S_7 which included 0, 1, 2, 4, and 7 pairs of serine mutations at "a", "d" positions, respectively (**Figure 1a,b**). To estimate the stability of these mutants, we used the CCBuilder 2.0 software package to calculate binding energy score of each specific CC (**Figure 1c**).[27] This package uses an empirical free-energy force field to predict binding between separate a-helical peptides, and we applied it to score the thermostability of our mutants. **Figure 1c** shows the Rosetta and Bristol University Docking Engine (BUDE) energy score of each CC sequence generated by CCBuilder 2.0 and confirms weakened interaction as a function of increasing the number of serine mutations. We also confirmed the CC library stability using AlphaFold2 structure prediction.[28] **Figure 1d** displays 3D rendering of CC serine mutants and predicts that CC-S_0, CC-S_1, CC-S_2, and CC-S_4 are folded as coiled-coils; in contrast, CC-S_7 fails to fold as a CC because of the missing hydrophobic interactions between the two a-helices (**Figure 1d, Figure S2**). Note that we also modeled CCs with stability that was weaker than CC-S_0 but greater than that of the CC-S_4 by introducing methionine pairs, displaying intermediate polarity, to evaluate CCs with a range of fine-tuned stabilities (**Figure S2, Table S1**). This data is not shown as the methionine mutants performed similarly in terms of predicted stability and cell response to their serine counterparts (**Figure S2**, **Figure S3**).

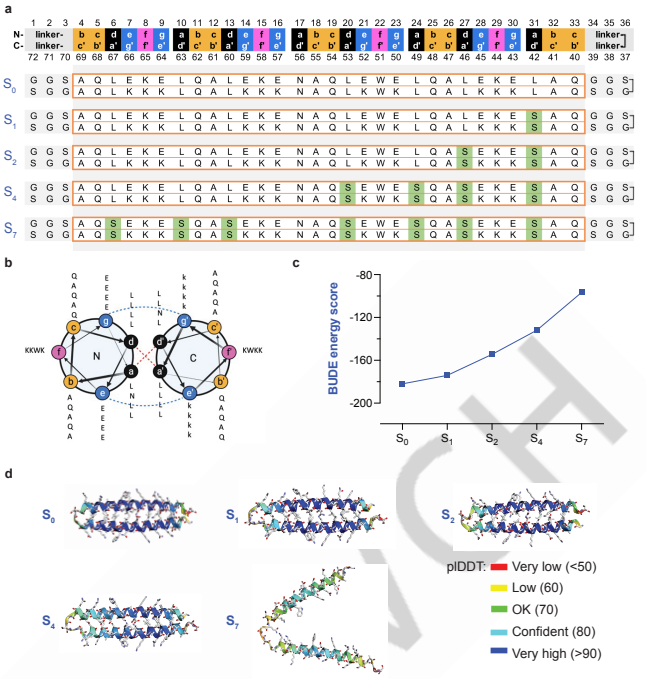

Figure 1. Molecular design of CC library based on folding energy and structure prediction. (a) Amino acid sequences of CC serine mutants. (b) CC-S_0 sequence shown in helical wheel diagram. Mutants were designed by replacing leucine to serine at "a", "d" positions. (c) BUDE energy score of CC serine mutants. (d) Illustration of predicted structures for CC-S_0, CC-S_1, CC-S_2, CC-S_4 and CC-S_7 using AlphaFold2. Confidence score for the prediction is color coded as shown in the legend at the bottom right. Values of 90 and greater are shown in dark blue and indicate high confidence in the predicted structure. plDDT =predicted local distance difference test.

Vinculin CCTSs Can be Engineered in a Predictable Manner to Detect Vinculin Tension

Clover and mRuby2 were chosen as the FRET pair of our CCTSs because of their large stokes shift, long Förster radius (R_0 =6.3 nm), and high photostability, allowing cellular imaging with a greater S/N.[29] Indeed, Hoffman and colleagues employed the Clover-mRuby2 pair to enhance the FRET response of the F40 analog GETS compared to mTFP1-venus pair.[30] We created CCTSs using the library of 72 aa CC domains shown in Figure 1 flanked by Clover/mRuby2. AlphaFold2 prediction of Clover-S_0-mRuby2 and Clover-S_7-mRuby2 confirmed that after the addition of Clover and mRuby2, CC domains fold the same structure as predicted without the FPs in **Figure 1d**, with slightly lower confidence score especially at the CC terminus (**Figure S4, Movie S1**). This validates that flanking CC domain with fluorescent proteins is not disruptive to S_0 folding, although slightly making the terminus of CC domain more flexible. CCTSs were inserted between the vinculin head (Vh) and tail (Vt) domains to create the TS constructs (**Scheme 1d, left**). As a force insensitive (Fi) control, we fused the CCTS at the C-terminus of full-length vinculin (**Scheme 1d, right**). In this control, vinculin tension is not transmitted to the CC and thus the FRET efficiency for the Fi provides the background signal independent of mechanical tension. In contrast, the CCTS inserted in the vinculin linker domain between Vh and Vt experiences forces which may

10.1002/anie.202407359

lead to unfolding and separation of the Clover/mRuby2 pair, causing decrease of FRET efficiency.

To quantify FRET, we measured the sensitized FRET index by acquiring donor emission, acceptor emission and sensitized FRET emission channels, segmenting FAs and performing image arithmetic on ~50-70 cells from n=5 experiments for each construct (see detailed workflow in **Figure S5**) (**Figure 2a**).[31],[32] S_0 displayed statistically similar FRET index values for the Fi control (23 ±2.7%) and TS (24 ±2.1%) constructs (**Figure 2b**). The lack of change in FRET between Fi and TS (*Δ*FRET) indicates that S_0 remains folded, thus vinculin tension fails to mechanically unfold CC-S_0 (**Figure 2c**). In contrast, the S_4 and S_7 constructs showed statistically similar low FRET values in both Fi (13.4 ±1.8% for S_4 and 12 ±1.5% for S_7) and TS (13.4 ±2.5% for S_4 and 13 ±2.7% for S_7). The FRET index was significantly greater for Fi and TS-S_0 constructs compared to that of S_4 and S_7. This demonstrates that S_4 and S_7 are considerably less stable and likely fail to adopt CCs within the cellular environment (**Figure 2a-c**). Interestingly, S_4 was predicted to adopt a stable CC structure by Alphafold2 (**Figure 1d**), but this was not observed in the cell environment, likely due to the fusion of Clover and mRuby2.

Intermediate stability CCs with S_1, and S_2 mutations showed significant ΔFRET values between TS and Fi constructs (**Figure 2a-c**). The FRET index of Fi-S_1 and S_2 were 24 ± 3.2%, and 24 ± 2.5%, respectively, which were comparable to FRET of CC-S_0 constructs, confirming that S_1 and S_2 are folded in the absence of external force. In contrast, the FRET index for TS-S_1 and S_2 were significantly reduced to 22±3.1% and 18±3.1%, respectively (**Figure 2b**). Note that the S_2 showed the greatest ΔFRET between TS and Fi constructs among the library of CCs investigated here (**Figure 2b,c**). TS-S_2 transfected MEF cells plated on poly-lysine (PL) surface are not able to spread, and the cells displayed uniform FRET index (25±1.3%) across the cell at levels similar to that observed in Fi constructs with stable CCs, confirming that the Fi controls represent a no adhesion state of the sensor (**Figure S6, Figure 2a,b**).

Because of the nature of CC folding, we expected an advantage of the CCTS is to provide a greater magnitude of FRET at rest compared to that of the ELP based opt-VinTS. To test this assumption, we expressed each construct in HEK293 and then measured FRET of the constructs in cell lysate. There is no force in these bulk solution experiments and hence the measurements provided the maximal FRET. LaCroix et al. reported that opt-VinTS with 42 aa and 0 aa linker length has a rest FRET efficiency ~55% and ~70% in cell lysate, respectively. The 42 aa opt-VinTS we tested showed FRET efficiency of 60 ±2.6%, which is similar to that reported by LaCroix et al. In contrast, TS-S_0 showed significantly greater resting FRET efficiency of 69 ±1.0% which is close to the rest FRET of 0 aa linker opt-VinTS (**Figure 2d**). This confirms that the antiparallel CC structure minimizes the distance between donor and acceptor, which increases S/N for the sensor. Note that FRET index was used in all our measurement to represent the relative value of FRET changes with the exception of the bulk FRET measurements conducted using a fluorometer using isolated tension sensors.

The live cell imaging results demonstrate TS-S_1 and TS-S_2 probes are partially unfolded by vinculin forces with the greater population of unfolded CCs for S_2, and thus confirming that S_2 offers the optimal sensitivity to detect vinculin tension. One of the unique features of using CC domains as tension sensors is their predicted step-like unfolding thermodynamically as well as in response to force.[24,33,34] This leads to a linear relationship between the fraction of unfolded probes in a region of interest and the FRET signal. To quantify the fraction of unfolded probes in our images, we set the FRET signal of Fi-S_0 as 0% unfolded and conversely, the Fi of S_7 as 100% unfolded. Intermediate FRET values between these extremes correspond to the percentage of unfolded CCs in each pixel. This linear relation is plotted in **Figure 2e** and then applied to cells transfected with Fi-S_2 and TS-S_2 (**Figure 2f**). The Fi-S_2 control showed that probes were uniformly folded, while TS-S_2 demonstrated an increasing fraction of open probe towards the edge of the cell in FAs and 20-70% of CCs unfolded mechanically within locations of FAs.

10.1002/anie.202407359

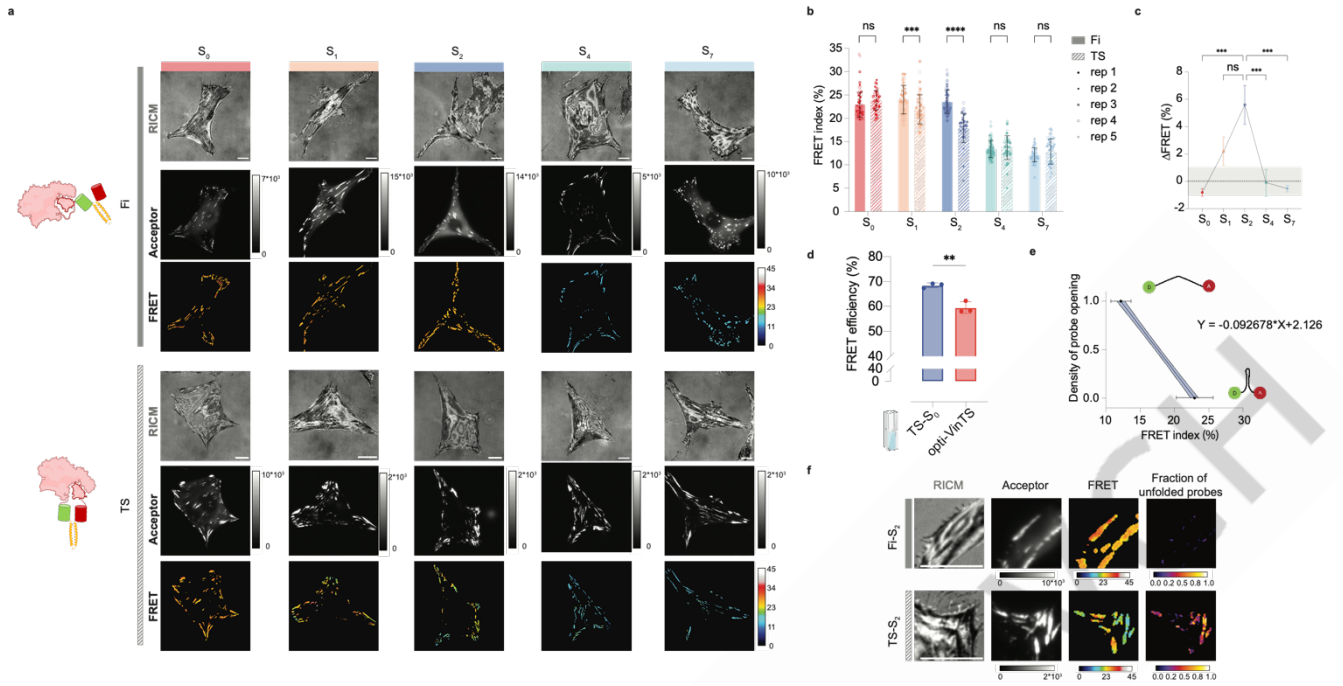

Figure 2. Ensemble FRET measurements in cell experiment. (a) RICM images (top), acceptor channel images (middle, gray), and FRET index images (bottom, RGB) of MEF cells expressed for CC library. Top three lanes of images demonstrate cells transfected with force insensitive constructs, and bottom three lanes of images indicate cells transfected with tension sensor constructs. The scale bar = 10 mm. (b) Quantification of FRET index comparing Fi and TS constructs among the CC library. Error bars represent SD. Each data represents an average FRET index of individual cell (n=58, 52, 78, 88, 55 for Fi and n =45, 67, 45, 54, 51 for TS, pooled from five individual experiments). *** p <0.001, **** p <0.0001, unpaired t-test, two-tailed, assuming equal SD. (c) Plot of ΔFRET for each sequence of CC library analyzed from a data set of (b). Δ FRET=$Mean_{Fi}$ - $Mean_{TS}$, mean data were analyzed from five individual experiment. Error bars represent SEM. *** p < 0.001, one-way ANOVA. (d) Quantification of FRET for TS-S_0 and opt-VinTS expressed in HEK 293 and collected from cell lysate (n=3). Error bars represent SD. SD=1.0% and 2.6%, respectively. p =0.0037, unpaired t-test, two-tailed, assuming equal SD. (e) Probability of probe opening considering P(Fi-S_0) =1, P(Fi-S_7) =0 (R^2 =0.8603, SD_{slope} =0.003542, $SD_{Y\text{-}intersept}$=0.01366). Error bars represent SD. Areas filled with blue represents 95% confidence intervals. Note that the goodness of fit was derived from the variance of the FRET values for the Fi-S_7 and Fi-S_0. (f) Representative FRET index images (left) converted to opening probe density (right) for Fi-S_2 and TS-S_2 using equation adopted from (e).

To further evaluate the impact of sequence variations on the unfolding dynamics of the coiled-coils (CCs) and to compare their relative unfolding energy, we performed steered molecular dynamics (SMD) simulations. In these simulations, we first solvated and equilibrated each CC within a water box and then applied force to a designated collective variable to break open the CC motif (**Figure 3a and Movie S2**). The collective variable is defined as the distance between the N and C termini mass centers (N-C distance), over which we can integrate to calculate the accumulated work needed to disrupt the CC. For each CC, we perform ten replicas of SMD simulations and combined the accumulated work according to Jarzynski Equality as the potential of mean force (PMF) of unfolding the CC.[35] A convergence test is performed to establish an appropriate number of replicas necessary for robust convergence (**Supplementary Note 2**).

Our simulations of the S_0, S_1, S_2, and S_4 CCs demonstrated a uniform trend: the accumulated work required to disrupt hydrophobic interactions increased monotonically up to an N-C distance of ~40 Å, after which it plateaued due to the complete opening of the CCs (**Figure 3b**). The corresponding force profiles for these variants increased from 0 pN to 60-75 pN initially and then sharply decreased at ~40 Å (**Figure S7a**). In contrast, S_7 exhibited a more gradual increase in PMF over the N-C distance and a significantly lower peak force. This deviation is likely due to the extensive mutations compromising the CC motif, preventing S_7 from maintaining its double helix structure, as indicated by FRET imaging (**Figure 2**).

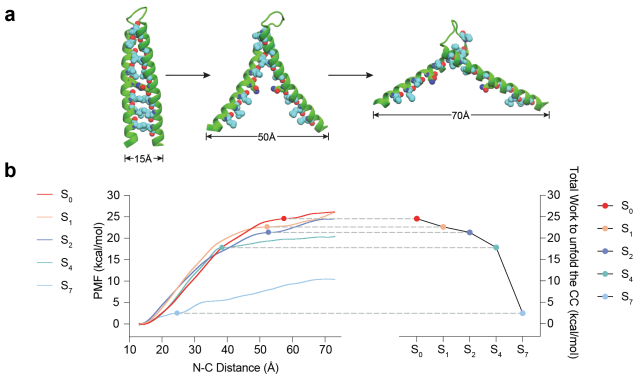

Figure 3. Steered molecular dynamics (SMD) predicts works required to unfold CCs. (a) Representative snapshots from a SMD simulation to unfold CC-S0, with increasing N-C distance (d =15, 50, 70Å). The protein is rendered in New

10.1002/anie.202407359

Cartoon, with residues on the coiled-coil interacting surface rendered in vDW representation. The carbon of LEU is in cyan and the carbon of ASN is in green. (b) The potential of mean force (PMF) as a function of N-C distance for CC library (left). The PMF is obtained by combining the accumulated works of 10 replicas of SMD simulations according to Jarzynski Equality. The data of all 10 replicas is shown in Figure S7. The total work needed to unfold each CC (right), measured as the potential energy of the point when the force drops to nearly 0 pN (<5 pN), is linearly decreasing as we increase the number of serine mutations.

Additionally, we determined the total work needed to unfold each CC, measured as the potential energy of the point when the force drops to nearly 0 pN (<5 pN). Our analysis across the CC variants revealed a descending order of unfolding work required: $S_0 > S_1 > S_2 > S_4 > S_7$. This trend is consistent with both BUDE energy score predictions (**Figure 1c**) and observations from our cellular assays (**Figure 2**). Remarkably, the introduction of serine mutations linearly reduced the unfolding work by approximately 8% per mutation pair, underscoring the tunability and predictability of CCs for engineering force-sensitive domains in genetically encoded tension sensors.

Force Calibration of CCs Reveals Thresholds of CCTSs

To measure the force required to unfold the CC structures, we conducted single molecule force spectroscopy on the S_0 and S_2 CCs using optical tweezers. Here, we trapped two micron-sized spheres using focused lasers and then the termini of the target molecule were coupled to each sphere using long, micron scale, DNA handles to avoid crosstalk between the lasers. We recombinantly expressed the CC proteins with an Avi-tag and Cys modification, at the N and C termini, respectively. Expressed proteins were confirmed to maintain alpha helical secondary structure through circular dichroism analysis (**Figure S8**). Subsequent biotinylation and Michael addition coupling generated CC constructs modified with N-terminal biotin and C-terminal transcyclooctyne (**Fig. 4a** and **Figure S9**). Separately we prepared a 2326 bp dsDNA "handle" with terminal tetrazine and azide groups. The CC protein and dsDNA handle were covalently linked via tetrazine-TCO click reaction, and then this protein-DNA chimera was grafted onto DBCO-modified polystyrene spheres (2.34 micron) using strain promoted azide-alkyne cycloaddition. The resulting protein-DNA-bead conjugate was then injected into a flow chamber where the N-terminal biotin on the CC bound to streptavidin (SA) on a 1.36-micron spheres (**Figure 4a**). Through optical manipulation of the beads, we simultaneously measured the force applied to each CC as well as the relative distance between the two beads, allowing us to track the length of the linker molecule as a function of force (**Figure 4b-e**). Large jumps in the distance were automatically identified using a changepoint algorithm (**Supplementary Note 3**) and indicated the force at which the target molecule underwent an opening or closing transition, depending on whether we stretched or relaxed the probe (**Figure 4d,e**, red and blue, respectively). This force against the distance measurement was plotted as a Force-Distance (F-D) curve (**Figure 4b-e**). The F-D curve of both CC-S_0 and CC-S_2 showed two states of structures fit by WLC with two contour lengths, indicating CC-S_0 and CC-S_2 will go through one major structural change upon the application of force, consistent with Gao et al.[24] Note that the transitions shown in **Figure 4d,e** show sharp transitions, confirming the digital nature of our probe. We repeated the stretch and relaxation cycles (50 nm/sec) to capture numerous unfolding and refolding events of CC-S_0 and CC-S_2 constructs, identified the force associated with each structural transition (**Figure 4d,e**), and histogrammed these forces (**Figure 4f,g**). The forces associated with stretching/relaxing motions are labeled as opening/closing forces, respectively, and all distributions were modeled as a Gaussian to facilitate comparison. The transition forces associated with refolding ($F_{refolding}$, depicted as blue lines in **Figure 4f,g**) showed narrow distributions for both S_0 and S_2 constructs ($F_{refolding}$-S_0 = 10.3 ± 0.59 pN and $F_{refolding}$-S_2 = 8.3 ± 0.69 pN, n=17 and 9, respectively). In contrast, the transition forces associated with unfolding ($F_{unfolding}$, depicted as red lines in **Figure 4f,g**) showed broader distributions with higher values ($F_{unfolding}$-S_0 = 14.7 ± 4.76 pN and $F_{unfolding}$-S_2 = 14.8 ± 3.02 pN, n=13 and 7, respectively). For the S_0 construct, we fit the data to a single Gaussian, however, the data may potentially fit a bimodal distribution of $F_{unfolding}$ (**Figure 4f**). Due to the limited number of data points, we avoided overfitting which would arise from using a bimodal distribution. The observed hysteresis and broadening between the unfolding and refolding force distributions (red and blue lines, **Figure 4f,g**) indicates that mechanical unfolding/refolding were under non-equilibrium conditions and involve energy dissipation, a well-documented phenomenon.[36-38] Importantly, the equilibrium unfolding force ($F_{1/2}$) for the CC constructs may be approximated as the intersection of the opening and closing force distributions.[39-41] In other words: the $F_{1/2}$ is the force at which the probe has equal probability of undergoing an opening or a closing transition. We calculated this "intersection of probabilities", yielding $F_{1/2}$ values of 11.6 and 9.9 pN for the S_0 and S_2 constructs, respectively (black dotted lines, **Figure 4f,g**). Because the distribution of closing force for both constructs is well-behaved and narrow, the range of possible intersections ($F_{1/2}$ values) is also small lending confidence to our approximation (**Supplementary Note 3**). The greater $F_{1/2}$ of S_0 compared to S_2 agrees with our modeling, where the total work to unfold S_0 is greater than that of S_2 and is also consistent with the cell FRET measurements that demonstrated greater ΔFRET for S_2 compared to that of S_0. Due to limited data at greater loading rates, the data was insufficient to fully model the threshold at zero force. Therefore, we focused our data analysis on calibrating the force threshold at 50 nm/sec loading rate, which is at the magnitude of vinculin physiological loading rate (in the order of 10 nm/sec).[42,43]

10.1002/anie.202407359

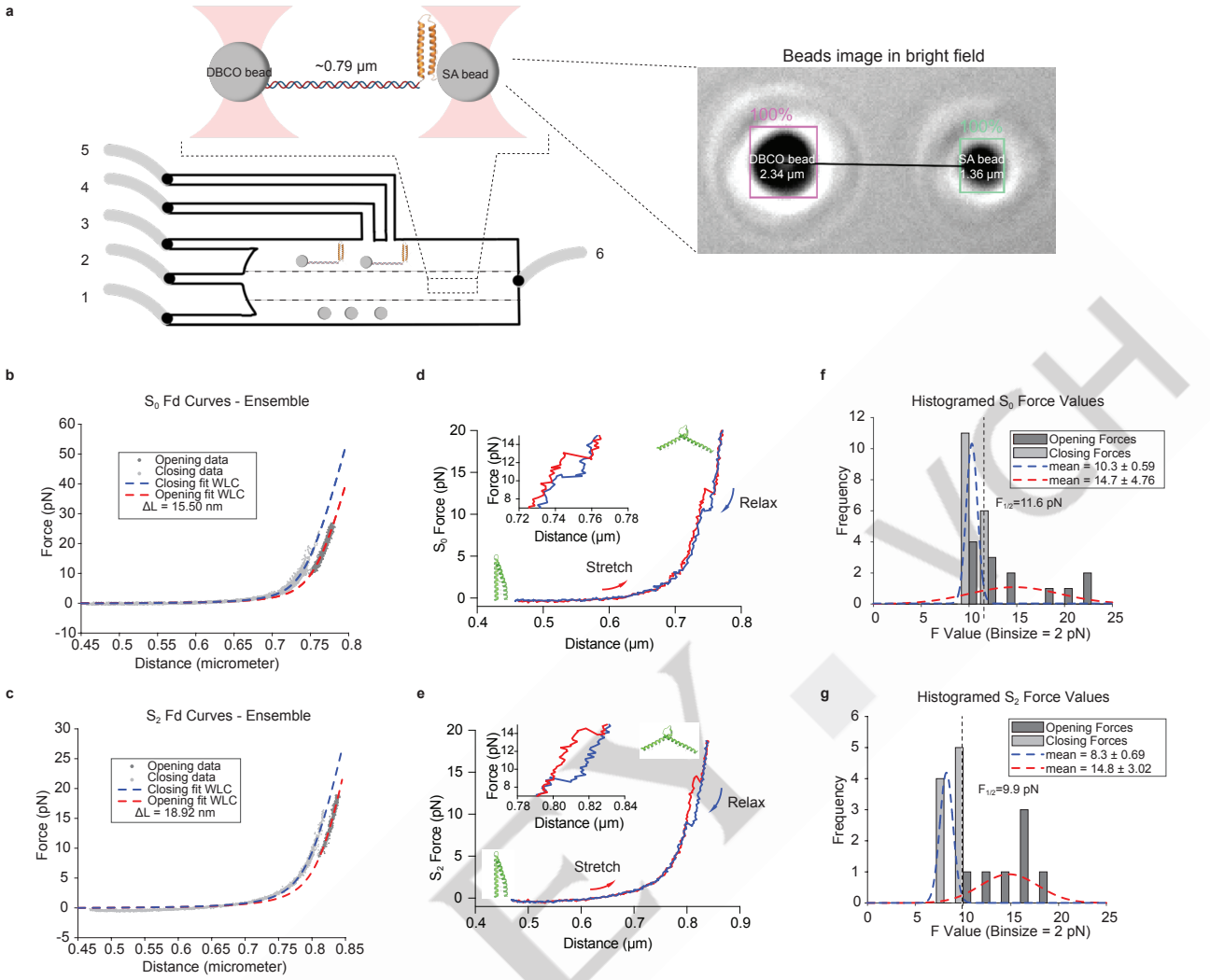

Figure 4. Single molecule force calibration of CC-S_0 and CC-S_2. (a) Illustration of optical tweezer set up with CC domain tethered between two polystyrene beads. A 2326 bp dsDNA is added as linker. Channel 1: SA beads in 1X PBS; channel 2, 4, and 5: 1X PBS; channel 3: DBCO beads incubated with CC-DNA in 1X PBS; channel 6: output to waste. (b,c) Ensemble F-D curves fit by WLC with closing and opening contour lengths for CC-S_0 and CC-S_2, respectively. The F-D unfolding and refolding curves for CC-S_0 and CC-S_2 constructs came from n =13 and 17 and n=7 and 9 trajectories, respectively. The loading rate was 50nm/sec. (d,e) Representative unfolding and refolding F-D curves for CC-S_0 and CC-S_2. (f,g) Histograms plotting the unfolding (red) and refolding forces (blue) for CC-S_0 and CC-S_2 with corresponding dotted lines depicting a Gaussian distribution based on the mean and standard deviation.

Analysis of CCTS data reveals dynamic sub-populations of vinculin experiencing F>9.9 pN

To investigate the dynamics of force evolution in vinculin during initial cell adhesion, we captured a timelapse video using the TS-S_2 ($F_{1/2}$ = 9.9 pN). Cells were seeded and imaged upon initial cell-surface encounter (t= 0 min) using a 5 min imaging interval. The cell adhesion area was small at t=0 min, as indicated by RICM, and this area had uniformly high FRET index (~0.28%), confirming that vinculin tension was <9.9 pN at this early timepoint (**Figure 5a**). As the cell spread and increased its adhesion area (t = 20 min), regions with low FRET values (~0.15%) were observed, indicating vinculin forces >9.9 pN in these regions, which is a greater magnitude force that could not be investigated in previous studies using the ELP construct with dynamic range of 1-6 pN.[4] From the timelapse video as well as kymograph analysis, regions with vinculin F>9.9 pN started from the edge of the cell and gradually expanded toward the center of the cell over the 60 min duration (**Figure 5a,b**). This enhancement in force magnitude and the appearance of elongated adhesions at the cell perimeter was consistent with FA maturation.[4] Histograms of single cell FRET values as a function of time (t=0, 30, 60 min) showed that the average FRET index decreased from 28% to 15% over this duration, which confirms maturation of adhesions and enhancement of tension signal (**Figure 5b**). The reversibility of CCTSs was further confirmed by treating cells with latrunculin B, an F-actin inhibitor, and observing an increase in FRET index (**Figure S10**).

We next wondered whether a small sub-population of vinculin proteins experience F>11.6 pN and unfold S_0. To answer this question, we performed pixel-by-pixel FRET analysis for n=50-70

cells that were cultured for 4 hrs on a glass substrate coated with fibronectin. Histograms and representative images of TS and Fi transfected MEF cells (S_0, S_1, and S_2) are shown in **Figure 5c**. We found that the Fi-S_0 construct had a FRET index value of 23 ± 2.7% and while the majority of the TS-S_0 constructs showed similar FRET values, there was a small population (0.4%) of vinculin that showed FRET values 3 standard deviations lower than the mean FRET for the Fi-S_0. This small shift is negligible statistically. It may be a result of a small fraction of vinculin that experiences sufficient force to unfold or alternatively it may be due to other parameters such as a change in donor-acceptor orientation which influences the kappa squared factor.[44] This sub-population of pixels with FRET values 3σ lower than the mean of their corresponding Fi construct grows to a more statically significant difference as the CC interaction becomes weaker (**Figure 5d**). For example, the percentage of pixels with FRET 3σ lower for S_1 =1%, and for S_2 =13%. Thus, we can infer that about 13% of vinculin in FAs experienced F >9.9 pN and nearly no vinculin experienced F >11.6 pN.

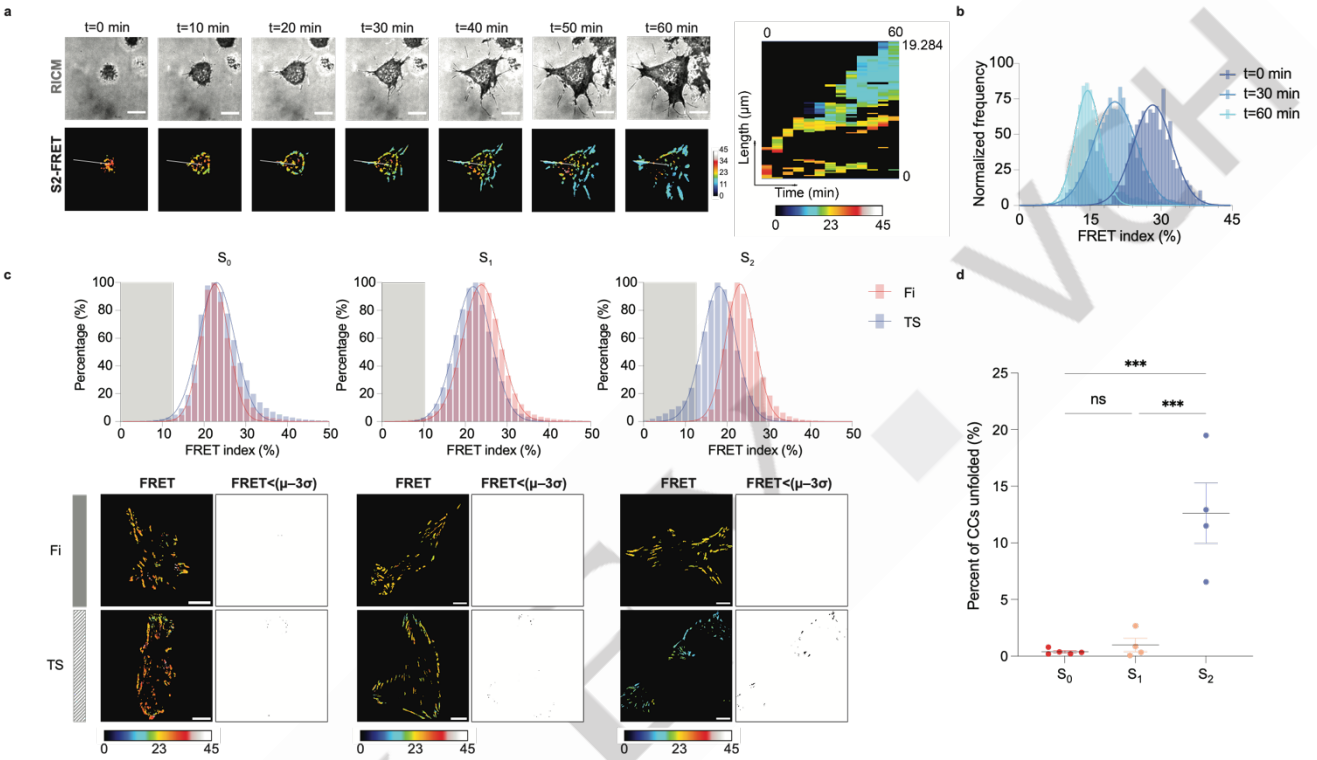

Figure 5. CCTS offers improved S/N for mapping vinculin tension in focal adhesions. (a) Time lapse video mapping vinculin tension using TS-S2 in RICM (top) and FRET (bottom) channels. The figure also shows a kymograph for the line scan indicated in the image. The scale bar = 10 mm. (b) Histogram analysis of single cell FRET from (a) as a function of time. For t =0 min the mean FRET= 28%, t =30 min mean FRET =20%, and for t =60 min mean FRET= 15%. (c) Pixel by pixel histogram analysis for FRET signal in cells expressing Fi-S_0, Fi-S_1 and Fi-S_2 (blue), TS-S_0, TS-S_1 and TS-S_2 (red) (bin size =4, gray area is where FRET TS <FRET Fiμ-3σ). The data was obtained from at least n =50 cells. Representative FRET and thresholded FRET<FRET μ-3σ binary images (black: FRET<FRETμ-3σ) for cells expressing Fi-S_0, Fi-S_1 and Fi-S_2 (top), TS-S_0, TS-S_1 and TS-S_2 (bottom). (d) Plot quantifying % of pixels with CCTS probes unfolded using the FRET > FRETμ-3σ for S_0, S_1 and S_2 (n=5,4 and 4, respectively). Error bars represent the SEM. SEM=0.11%, 0.60% and 2.67%, respectively. *** p <0.001, ns p=0.9520, one-way ANOVA.

Conclusion

We have demonstrated that CCs represent a tunable force-responsive element that undergoes a binary structural transition upon experiencing a threshold external force. The CC domain can be programmed using well established factors including the length of hydrophobic surface, the hydrophobicity of the residues in the hydrophobic core, as well as peptide geometry. The relative mechanical stability of CCs can be predicted by a number of approaches including CCBuilder thermodynamic analysis, AlphaFold2 and SMD simulations. In our hands, these computational tools generally showed good agreement with the cell experiments with the exception of CC-S_4 which was unstable in cells but was predicted to fold based on CCBuilder and AlphaFold2 modeling. This discrepancy is likely because our modeling methods based on CCBuilder and AlphaFold2 do not introduce loading rate and CC alpha helical structure was restrained in our SMD simulation, which will likely result in relatively more stable CC interactions overall compared to that found in the cell environment.[45] Additionally, SMD employs ultrafast loading rates (in our case this was 1.5×10^7 nm/s) compared to physiological and experimental values which suggests that SMD is better suited to compare the relative mechanical stability of different CCs rather than to obtain absolute

10.1002/anie.202407359

information on individual CC unfolding. Furthermore, the S_4 is at the cusp of transitioning between the folded and unfolded states, and factors such as the fusion of FPs and the cell environment at 37 ºC may contribute to destabilizing the CC-S_4 in cells.

The vinculin CCTSs revealed force distributions in cells in a temporarily and spatially defined manner. Importantly, cell FRET analysis showed that the vast majority of vinculin experiences F <9.9 pN upon initial cell adhesion but then following cell spreading and formation of more stable adhesions led to a substantial population of vinculin with *F* >9.9 pN. Furthermore, CCTS facilitates quantification of sub-populations of vinculin experiencing threshold magnitudes of tension. For example, in fully spread cells 13% of vinculin experienced F >9.9 pN but less than 0.5% showed F>11.6 pN. These magnitudes represent greater forces than had previously been reported by Grashoff et al. where they concluded vinculin tension of 1-6 pN.[4] The random coil GETS display weak sensitivity when F>6 pN and this likely explains the different magnitudes of force reported. Our measured vinculin forces, however, are consistent with force spectroscopy showing the vinculin F-actin bonds are maximally stable at 8 pN.[46]

In conclusion, the tunable threshold binary force response of CCTS represents a powerful feature of this class of probe that will facilitate the investigation of mechanosensitive proteins in living systems. Given that the analog GETS have been used to investigate mechanobiology of many cell types[47-49] including primary cells and stem cells, as well as more complex organisms[50], we anticipate that the CCTS will likely find similar utility. Moreover, the programmability will help boost S/N and fine tune the sensor for specific applications in mind.

One potential weakness of the CCTS design is that the long length of the 72aa CC may perturb the POI function when fully extended and ideally shorter sensors would be more desirable. Such truncated CCs will be a future area of investigation.

Secondly, greater magnitudes of ΔFRET would be desirable as this would lead to enhanced S/N for the sensor. This requires protein engineering of alternate types of fluorescence reporters or technical improvements in FRET measurements. For example, an orange light-absorbing chromoprotein named ShadowR is a novel FLIM-FRET dark acceptor for pairing with mScarlet or mRuby2, which are expected to produce a more significant FRET change in response to forces within CCTSs.[51] Lastly, CC will likely form condensates in either unzipping geometry (antiparallel) or sheering geometry (parallel) if the target protein is not organized in a “polarized” manner and this is a requirement to avoid the previously reported condensation of CCs.[23] Another technical difficulty is the accuracy and the throughput of the calibration of the force threshold of CC motif. Here we reported the $F_{1/2}$ of CC-S_0 and CC-S_2 to be 11.6 and 9.9 pN, respectively, using recombinantly expressed CC domains. Our measurements likely do not capture the complex behavior of coiled-coils within the *in vivo* cellular environment where protein-protein interactions and molecular crowding could influence unfolding responses. Furthermore, experimentally calibrating each individual sequence of CC is limited by low throughput single molecule force calibrations, which result in limited data points or slow screening of large libraries of CCs. These difficulties can be addressed by improved investigation of the accuracy of molecular dynamics simulation, which may possibly recapitulate *in vivo* conditions as well as *de novo* peptides.

Looking forward, it does not escape us that CCTSs can be engineered with additional capabilities. For example, CC can be programmed to trigger protein-protein binding and functional responses following mechanical unfolding. Such functional responses may allow for integration of synthetic biology circuits that are triggered mechanically.[52] [53]

Acknowledgements

We would like to thank Dr. A. Mattheyses for kindly sharing some of their plasmids that were used in this work; Dr. A. Garcia for kindly providing the vinculin null cell line; Dr. O. Laur at Emory cloning core for constructing some of the plasmids in this work; Dr. J.C. Gumbart for scientific input and advice on SMD work. K.Salaita acknowledges financial support from NIH NIAID R01AI172452 and NIGMS 1RM1GM145394.

Keywords: biophysics • protein engineering • biosensors • FRET

[1] K. H. Vining, D. J. Mooney, *Nat Rev Mol Cell Biol* **2017**, *18*, 728-742.
[2] J. R. Lange, B. Fabry, *Exp Cell Res* **2013**, *319*, 2418-23.
[3] A. Matamoro-Vidal, R. Levayer, *Curr Biol* **2019**, *29*, R762-R774.
[4] C. Grashoff, B. D. Hoffman, M. D. Brenner, R. Zhou, M. Parsons, M. T. Yang, M. A. McLean, S. G. Sligar, C. S. Chen, T. Ha, M. A. Schwartz, *Nature* **2010**, *466*, 263-266.
[5] D. R. Stabley, C. Jurchenko, S. S. Marshall, K. S. Salaita, *Nat Methods* **2011**, *9*, 64-7.
[6] Y. Liu, K. Yehl, Y. Narui, K. Salaita, *J Am Chem Soc* **2013**, *135*, 5320-3.
[7] K. Galior, Y. Liu, K. Yehl, S. Vivek, K. Salaita, *Nano Letters* **2016**, *16*, 341-348.
[8] A. Freikamp, A. L. Cost, C. Grashoff, *Trends Cell Biol* **2016**, *26*, 838-847.
[9] P. Ringer, A. Weissl, A. L. Cost, A. Freikamp, B. Sabass, A. Mehlich, M. Tramier, M. Rief, C. Grashoff, *Nat Methods* **2017**, *14*, 1090-1096.
[10] F. Meng, T. M. Suchyna, F. Sachs, *FEBS J* **2008**, *275*, 3072-87.
[11] Y. Zhang, C. Ge, C. Zhu, K. Salaita, *Nat Commun* **2014**, *5*, 5167.
[12] S. J. Tan, A. C. Chang, S. M. Anderson, C. M. Miller, L. S. Prahl, D. J. Odde, A. R. Dunn, *Science Advances* **2020**, *6*, eaax0317.
[13] H. Matsubara, H. Fukunaga, T. Saito, K. Ikezaki, M. Iwaki, *ACS Nano* **2023**, *17*, 13185-13194.
[14] R. Roy, S. Hohng, T. Ha, *Nature Methods* **2008**, *5*, 507-516.
[15] K. Austen, P. Ringer, A. Mehlich, A. Chrostek-Grashoff, C. Kluger, C. Klingner, B. Sabass, R. Zent, M. Rief, C. Grashoff, *Nat Cell Biol* **2015**, *17*, 1597-606.
[16] D. N. Woolfson, *Adv Protein Chem* **2005**, *70*, 79-112.
[17] A. Ljubetic, F. Lapenta, H. Gradisar, I. Drobnak, J. Aupic, Z. Strmsek, D. Lainscek, I. Hafner-Bratkovic, A. Majerle, N. Krivec, M. Bencina, T. Pisanski, T. C. Velickovic, A. Round, J. M. Carazo, R. Melero, R. Jerala, *Nat Biotechnol* **2017**, *35*, 1094-1101.

[18] P. Lopez-Garcia, M. Goktas, A. E. Bergues-Pupo, B. Koksch, D. Varon Silva, K. G. Blank, *Phys Chem Chem Phys* **2019**, *21*, 9145-9149.
[19] W. D. Kohn, C. M. Kay, R. S. Hodges, *Protein Sci* **1995**, *4*, 237-50.
[20] M. Goktas, C. Luo, R. M. A. Sullan, A. E. Bergues-Pupo, R. Lipowsky, A. Vila Verde, K. G. Blank, *Chem Sci* **2018**, *9*, 4610-4621.
[21] M. Goktas, K. G. Blank, *Advanced Materials Interfaces* **2017**, *4*.
[22] T. Bornschlögl, M. Rief, *Physical Review Letters* **2006**, *96*, 118102.
[23] Y. Ren, J. Yang, B. Fujita, H. Jin, Y. Zhang, J. Berro, *Science Advances* **2023**, *9*, eadi1535.
[24] Y. Gao, G. Sirinakis, Y. Zhang, *Journal of the American Chemical Society* **2011**, *133*, 12749-12757.
[25] T. Bornschlögl, M. Rief, *Langmuir* **2008**, *24*, 1338-1342.
[26] H. Witt, A. Janshoff, in *SNAREs: Methods and Protocols* (Ed.: R. Fratti), Springer New York, New York, NY, **2019**, pp. 145-159.
[27] C. W. Wood, D. N. Woolfson, *Protein Science* **2018**, *27*, 103-111.
[28] M. Mirdita, K. Schütze, Y. Moriwaki, L. Heo, S. Ovchinnikov, M. Steinegger, *Nature Methods* **2022**, *19*, 679-682.
[29] A. J. Lam, F. St-Pierre, Y. Gong, J. D. Marshall, P. J. Cranfill, M. A. Baird, M. R. McKeown, J. Wiedenmann, M. W. Davidson, M. J. Schnitzer, R. Y. Tsien, M. Z. Lin, *Nat Methods* **2012**, *9*, 1005-12.
[30] A. S. LaCroix, A. D. Lynch, M. E. Berginski, B. D. Hoffman, *eLife* **2018**, *7*, e33927.
[31] J. van Rheenen, M. Langeslag, K. Jalink, *Biophysical Journal* **2004**, *86*, 2517-2529.
[32] U. Horzum, B. Ozdil, D. Pesen-Okvur, *MethodsX* **2014**, *1*, 56-59.
[33] D. Krylov, I. Mikhailenko, C. Vinson, *The EMBO Journal* **1994**, *13*, 2849-2861.
[34] H. Qian, *Biophys J* **1994**, *67*, 349-55.
[35] C. Jarzynski, *Physical Review Letters* **1997**, *78*, 2690-2693.
[36] J. Liphardt, S. Dumont, S. B. Smith, I. Tinoco, C. Bustamante, *Science* **2002**, *296*, 1832-1835.
[37] D. Collin, F. Ritort, C. Jarzynski, S. B. Smith, I. Tinoco, C. Bustamante, *Nature* **2005**, *437*, 231-234.
[38] S. Raman, T. Utzig, T. Baimpos, B. Ratna Shrestha, M. Valtiner, *Nature Communications* **2014**, *5*, 5539.
[39] A. Mossa, M. Manosas, N. Forns, J. M. Huguet, F. Ritort, *Journal of Statistical Mechanics: Theory and Experiment* **2009**, *2009*, P02060.
[40] A. Alemany, F. Ritort, *The Journal of Physical Chemistry Letters* **2017**, *8*, 895-900.
[41] T. Naranjo, K. M. Lemishko, S. de Lorenzo, Á. Somoza, F. Ritort, E. M. Pérez, B. Ibarra, *Nature Communications* **2018**, *9*, 4512.
[42] A. Y. Alexandrova, K. Arnold, S. Schaub, J. M. Vasiliev, J. J. Meister, A. D. Bershadsky, A. B. Verkhovsky, *PLoS One* **2008**, *3*, e3234.
[43] V. Swaminathan, J. M. Kalappurakkal, S. B. Mehta, P. Nordenfelt, T. I. Moore, N. Koga, D. A. Baker, R. Oldenbourg, T. Tani, S. Mayor, T. A. Springer, C. M. Waterman, *Proc Natl Acad Sci U S A* **2017**, *114*, 10648-10653.
[44] B. W. van der Meer, *Reviews in Molecular Biotechnology* **2002**, *82*, 181-196.
[45] M. Goktas, C. Luo, R. M. A. Sullan, A. E. Bergues-Pupo, R. Lipowsky, A. Vila Verde, K. G. Blank, *Chemical Science* **2018**, *9*, 4610-4621.
[46] D. L. Huang, N. A. Bax, C. D. Buckley, W. I. Weis, A. R. Dunn, *Science* **2017**, *357*, 703-706.
[47] F. Li, A. Chen, A. Reeser, Y. Wang, Y. Fan, S. Liu, X. Zhao, R. Prakash, D. Kota, B.-Y. Li, H. Yokota, J. Liu, *Scientific Reports* **2019**, *9*, 5615.
[48] L. Sigaut, C. von Bilderling, M. Bianchi, J. E. Burdisso, L. Gastaldi, L. I. Pietrasanta, *Scientific Reports* **2018**, *8*, 9788.
[49] M. J. Paszek, C. C. DuFort, O. Rossier, R. Bainer, J. K. Mouw, K. Godula, J. E. Hudak, J. N. Lakins, A. C. Wijekoon, L. Cassereau, M. G. Rubashkin, M. J. Magbanua, K. S. Thorn, M. W. Davidson, H. S. Rugo, J. W. Park, D. A. Hammer, G. Giannone, C. R. Bertozzi, V. M. Weaver, *Nature* **2014**, *511*, 319-325.
[50] M. Krieg, A. R. Dunn, M. B. Goodman, *Nature Cell Biology* **2014**, *16*, 224-233.
[51] H. Murakoshi, H. Horiuchi, T. Kosugi, M. Onda, A. Sato, N. Koga, J. Nabekura, *Scientific Reports* **2019**, *9*, 12072.
[52] D. C. Sloas, J. C. Tran, A. M. Marzilli, J. T. Ngo, *Nature Biotechnology* **2023**, *41*, 1287-1295.
[53] J. H. Choe, P. B. Watchmaker, M. S. Simic, R. D. Gilbert, A. W. Li, N. A. Krasnow, K. M. Downey, W. Yu, D. A. Carrera, A. Celli, J. Cho, J. D. Briones, J. M. Duecker, Y. E. Goretsky, R. Dannenfelser, L. Cardarelli, O. Troyanskaya, S. S. Sidhu, K. T. Roybal, H. Okada, W. A. Lim, *Science Translational Medicine* **2021**, *13*, eabe7378.

10.1002/anie.202407359

Table of Contents

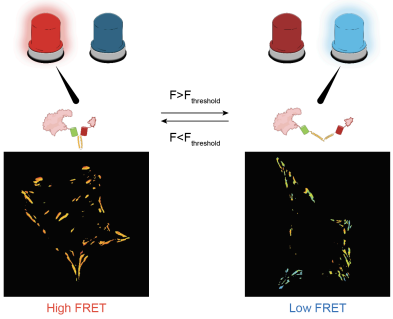

Here, we create a genetically-encoded force probe by engineering a coiled-coil domain flanked by fluorescent proteins that undergo FRET. These probes are fully tunable and calibrated by modeling and single molecule force spectroscopy and allow one to measure forces within living systems.